FEDSM2024-130651

SPARSE REDUCED-ORDER MODELING OF A HOVERING HAWKMOTH'S WAKE

Seth Lionetti¹, Tyson L. Hedrick², Chengyu Li¹

¹ Villanova University, Villanova, PA 19085, USA

² University of North Carolina at Chapel Hill, Chapel Hill, NC 27599, USA

ABSTRACT

As insects fly, their wings generate complex wake structures that play a crucial role in their aerodynamic force production. This study focuses on utilizing reduced order modeling techniques to gain valuable insights into the fluid dynamic principles underlying insect flight. Specifically, we used an immersed-boundary-method-based computational dynamics (CFD) solver to simulate a hovering hawkmoth's wake, and then identified the most energetic modes of the wake using proper orthogonal decomposition (POD). Furthermore, we employed a sparse identification of nonlinear dynamics (SINDy) approach to find a simple reduced order model that relates the most energetic POD modes. Through this process, we formulated multiple different models incorporating varying numbers of POD modes. To compare the accuracy of these models, we utilized a force survey method to estimate the aerodynamic forces produced by the hawkmoth's wings. This force survey method uses an impulse-based approach to calculate the aerodynamic lift and drag based solely on the velocity and vorticity information provided by the model. By comparing the estimated aerodynamic force with the actual force production calculated by the CFD solver, we were able to find the simplest model that still provides an accurate representation of the complex wake produced by the hovering hawkmoth wings. We also evaluated the stability and accuracy of this model as the number of flapping cycles increases with time. The reduced order modeling of insect flight has important implications for the design and control of bio-inspired micro-aerial vehicles. In addition, it holds the potential to reduce the computational cost associated with high-fidelity CFD simulations of complex flows.

NOMENCLATURE

Velocity components
Pressure
Reynolds number
Cycle-averaged wingtip velocity
Average wing chord length
Kinematic viscosity of air
i th POD mode
i th POD coefficient
Total number of POD modes
Number of POD modes used in SINDy model
SINDy input data
SINDy candidate function library
SINDy sparse coefficient matrix
Flapping frequency
Vorticity

1. INTRODUCTION

As insects fly, their wings produce complex wake structures that play a role in their aerodynamic force production [1, 2]. However, experiments and computational simulations of insect flight can be time consuming, computationally intensive, and difficult to analyze due to their many degrees of freedom. One potential solution to these problems is reduced order modelling. Reduced order modeling can be used to derive a simple dynamic model for complex flow phenomena [3, 4]. In addition, reduced order models of insect flight can provide insights into the

underlying dynamics involved in flapping-wing propulsion, as well as significantly reduce the computational complexity associated with simulating insect flight.

Developing a reduced order model often requires decomposing the flow field into a group of time-varying modes. Proper Orthogonal Decomposition (POD) is one commonly used decomposition method [5, 6]. The benefit of POD is that it effectively transforms the complex flow into a compact coordinate system that can be used to create a reduced-order model. One common technique for reduced-order modeling is Galerkin Projection, wherein the governing equations are projected onto the POD modes. Alternatively, data-driven algorithms such as Sparse Identification of Nonlinear Dynamics (SINDy) can be used to identify reduced order models using only the flow data, without relying on the governing equations. The goal of SINDy is to use sparse regression to identify a system of simple and interpretable dynamic equations capable of describing complex phenomena [7, 8].

Previous applications of SINDy in fluid mechanics have largely focused on canonical problems, such as flow over a cylinder [9, 10]. In this study, we apply SINDy to the more complex flow produced by a hovering hawkmoth's wings. We first simulate a hovering hawkmoth's wake using an in-house computational fluid dynamics (CFD) solver. Then, we use POD to decompose the flow into a set of time-varying modes. A simple reduced order model relating these modes is created using SINDy. Finally, to evaluate the accuracy of the model, we compare its prediction of the hawkmoth's aerodynamic force generation against our initial simulation results.

2. METHODOLOGY

2.3 Governing equations and numerical method

To simulate the aerodynamic wake of a hovering hawkmoth, we employ an in-house immersed-boundary-method-based computational fluid dynamics solver. The solver is used to solve the three-dimensional viscous incompressible time-dependent Navier Stokes equations that govern the flow. The nondimensional form of these equations is shown below:

$$\frac{\partial u_{i}}{\partial x_{i}} = 0;$$

$$\frac{\partial u_{i}}{\partial t} + \frac{\partial (u_{i}u_{j})}{\partial x_{i}} = -\frac{\partial p}{\partial x_{i}} + \frac{1}{Re} \frac{\partial}{\partial x_{i}} (\frac{\partial u_{i}}{\partial x_{i}})$$
(1)

where U_i (i=1, 2, 3) and p are the velocity components and pressure, respectively. The Reynolds number, given by $Re = \frac{\overline{U_{tip}} c}{v}$ (where $\overline{U_{tip}}$ is the cycle-averaged wingtip velocity, c is the average wing chord length, and v is the kinematic viscosity of air), is equal to 7335.

The governing equations are discretized in space using a cell-centered collocated arrangement of the primitive variables and are evaluated using a second-order central difference scheme. A fractional step method is used to integrate the equations in time. Boundary conditions are imposed on the immersed boundaries (in this case, the hawkmoth's flapping

wings) via a ghost cell procedure, which eliminates the need for computationally intensive remeshing algorithms. Validations and additional details related to this computational method can be found in our previous studies [11-15]. Our flow solver has been successfully utilized in studies of flapping flight [16-20].

2.4 Proper orthogonal decomposition

Proper orthogonal decomposition (POD) is applied to the simulation results to decompose the flow into a set of time-varying modes. The temporal fluctuation of each mode Φ_i is given by its associated coefficient α_i . The flow field at any point in time can therefore be expressed as a linear superposition of POD modes:

$$U(x,t) = \overline{U} + \sum_{i=1}^{M} \alpha_i(t) \, \Phi_i(x) \tag{2}$$

where \overline{U} is the mean flow and M is the total number of modes.

The POD algorithm employed in this study is known as the method of snapshots [5]. A sequence of snapshots is created by sampling the flow at S instances throughout the hawkmoth's flapping cycle. The resulting snapshot matrix W has rows containing the velocity components at each grid point and S columns corresponding to the total number of snapshots. Then, the autocovariance matrix $A = W^T W$ is used to solve the eigenvalue problem $AV_i = \lambda_i V_i$. Finally, the POD modes are given by $\Phi_i = \frac{1}{\sqrt{\lambda_i}} \sum_{j=1}^S (V_i)_j (W - \overline{U})$.

One benefit of modal decomposition algorithms such as POD is their ability to greatly reduce the dimensionality of complex flow phenomena. Using the aforementioned method of snapshots, the number of degrees of freedom necessary to represent a hovering hawkmoth's wake is reduced to just 96 (corresponding to a total of M=96 POD modes). Modes are ordered according to their contribution towards the total kinetic energy of the flow, such that lower modes (Φ_1 , Φ_2 , Φ_3 , etc.) are significantly more energetic than higher modes. For this reason, it is likely that only a small subset of the 96 POD modes is required to accurately model a hawkmoth's wake.

2.4 Sparse Identification of Nonlinear Dynamics

Next, we use Sparse Identification of Nonlinear Dynamics (SINDy) to formulate a reduced order model of the hovering hawkmoth's wake. In this study, the input data for SINDy consists of the temporal coefficients α_i corresponding to the first N POD modes. Then, sparse regression is performed on the system shown in equation (3).

$$\dot{X} = \Theta(X) \Xi \tag{3}$$

The matrix X contains the input data, and \dot{X} is its time derivative. $\Theta(X)$ contains a library of candidate polynomials for the model. In this study, we employ candidate polynomials up to order 3. Ξ is the sparse coefficient matrix that denotes which columns of theta are active. SINDy utilizes sparsity promotion to force as many of these coefficients to zero as possible, resulting in the simplest model that accurately describes the system. The model we obtain using the SINDy algorithm takes

the form of a dynamical system relating the *N* most energetic POD modes. Figure 6 shows a schematic of the SINDy algorithm employed in this study.

2.4 Force Survey Method

To evaluate the accuracy of the SINDy model, we employ a force survey method (FSM) to calculate the lift and drag produced by the hawkmoth's wings. Because the model does not include any pressure information, FSM is required to calculate the aerodynamic forces using only the velocity components predicted by the model. This method is based on the impulse equation first published by Noca et al. [21]:

equation first published by Noca et al. [21]:

$$\vec{F} = -\frac{1}{N-1} \frac{d}{dt} \int_{V(t)} \vec{r} \times \vec{\omega} dV + \oint_{S(t)} \vec{n} \cdot \gamma_{imp} dS$$

$$+ \frac{1}{N-1} \frac{d}{dt} \oint_{S_b(t)} \vec{r} \times (\vec{n} \times \vec{u}) dS - \oint_{S_b(t)} \vec{n} \cdot (\vec{u} - \vec{u}_S) \vec{u} dS$$

$$\gamma_{imp} = \frac{1}{2} u^2 I - \vec{u} \vec{u} - \frac{1}{N-1} (\vec{u} - \vec{u}_S) (\vec{r} \times \vec{\omega}) + \frac{1}{N-1} \vec{\omega} (\vec{r} \times \vec{u})$$

$$+ \frac{1}{N-1} [\vec{r} \cdot (\nabla \cdot T) I - \vec{r} (\nabla \cdot T)] + T$$
(4)

Validations and additional details related to the force survey method can be found in previous studies [22, 23].

3. RESULTS AND DISCUSSION

Using the results from the CFD simulation, we can examine the aerodynamic performance of the hovering hawkmoth. Figure 1 shows the Q-criterion wake structures produced by the hawkmoth's flapping wings during the middle of the downstroke and the middle of the upstroke. The wake is shed directly below the hawkmoth's body. In addition, we observe that during the downstroke, a large leading-edge vortex is formed along the hawkmoth's wings.

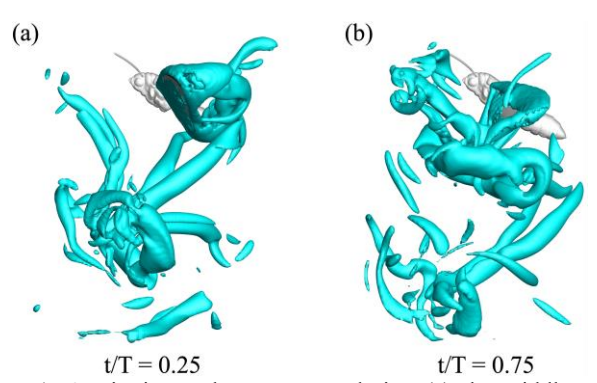


Figure 1. Q-criterion wake structures during (a) the middle of the downstroke and (b) the middle of the upstroke.

Previous studies have shown that vortices and wake structures produced during insect flight play a significant role in the insect's aerodynamic performance [1, 2]. Figure 2 shows the lift (vertical force) and drag (horizontal force) generated by one of the hawkmoth's wings during one flapping cycle. Lift is mainly generated during the downstroke, which occurs during the first half of the flapping cycle. Some lift is also produced during the upstroke. Positive drag is generated during the downstroke, and negative drag is generated during the upstroke.

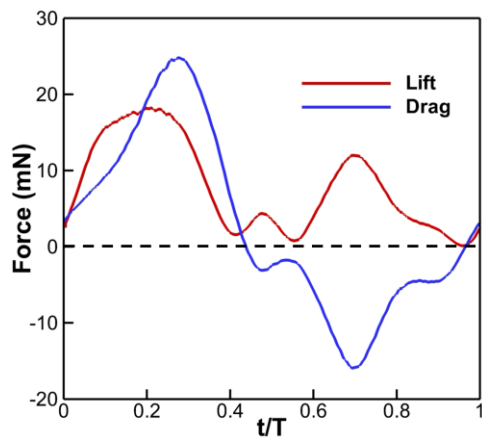


Figure 2. Instantaneous aerodynamic force production by one of the hawkmoth's wings during one flapping cycle.

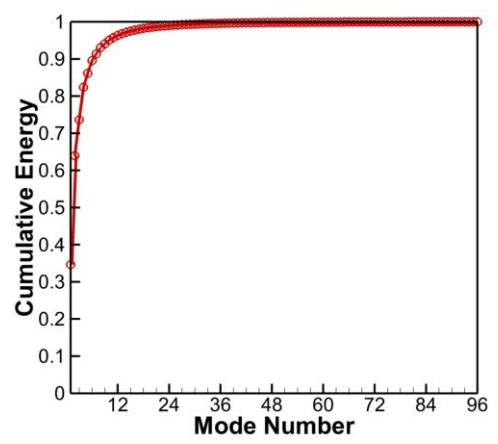


Figure 3. Cumulative energy contribution by the 96 POD modes. Energy is shown as a fraction of the total kinetic energy of the flow.

Table 1. Contribution of the first 8 POD modes towards the total kinetic energy.

	Contribution Accumulation		
Mode	(%)	(%)	
1	34.6	34.6	
2	29.4	64.0	
3	9.63	73.6	
4	8.76	82.4	
5	3.77	86.2	
6	3.42	89.6	
7	1.79	91.4	
8	1.70	93.1	

As demonstrated in Figure 1, the wake produced by the hovering hawkmoth's wings is complex, which makes formulating a simple model for the wake challenging. POD is therefore used to reduce the degrees of freedom of the flow to include just 96 time-varying modes. Figure 3 and Table 1 show the cumulative energy contributions of these modes towards the

total kinetic energy of the wake. The first eight contribute over 90% of the total energy. In addition, the first six modes are depicted in Figure 4, and the parametric relationships between their respective coefficients are shown in Figure 5. Interpreting the Lissajous curves in Figure 5 reveals there is a roughly harmonic relationship between the modes. We also observe that the modes occur in pairs that oscillate with the same frequency. For example, α_1 and α_2 fluctuate at a frequency equal to the hawkmoth's flapping frequency (f = 25.6 Hz). Similarly, α_3 and α_4 fluctuate at 2f, α_5 and α_6 fluctuate at 3f, etc. Table 1 shows that the modes in each "mode pair" also contribute roughly the same proportion of the total kinetic energy.

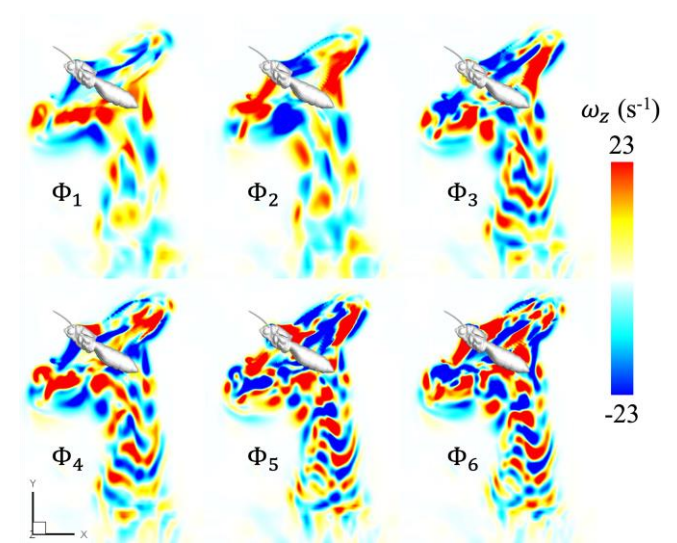


Figure 4. Vorticity (ω_z) contours for the first six POD modes $(\Phi_1$ to $\Phi_6)$.

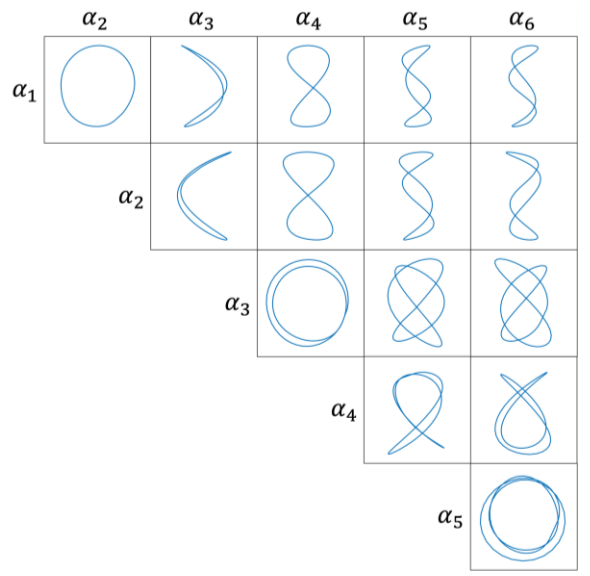


Figure 5. Lissajous curves showing the parametric relationships between the first six POD coefficients (α_1 to α_6).

The POD modes provide a convenient coordinate system that can be used to formulate a reduced order model of the hawkmoth's wake. A schematic of the SINDy algorithm used to create the model is shown in Figure 6, using just the first two modes (α_1 and α_2) as an example. In this figure, the identified system does a relatively good job of capturing the real relationship between these modes. However, Table 1 shows that the first two modes contribute only 64% of the total kinetic energy of the flow. To create a model that captures over 90% of the total kinetic energy, we instead use the first eight POD coefficients as inputs for the SINDy algorithm. The resulting model is shown in equation (5):

$$\dot{\alpha}_{1} = 6.7947 \alpha_{2}
 \dot{\alpha}_{2} = -5.7256 \alpha_{1}
 \dot{\alpha}_{3} = 12.8693 \alpha_{4}
 \dot{\alpha}_{4} = -12.0264 \alpha_{3}
 \dot{\alpha}_{5} = 19.1913 \alpha_{6}
 \dot{\alpha}_{6} = -17.9167 \alpha_{5}
 \dot{\alpha}_{7} = 25.0649 \alpha_{8}
 \dot{\alpha}_{8} = -24.2253 \alpha_{7}$$
(5)

Due to the sparsity promotion involved in SINDy, the above reduced order model is both simple and interpretable. Although the candidate function library contains polynomial functions up to order three, each equation in the model system includes just one first-order term. In addition, the dynamics of each mode depend solely on its complementary mode in the "mode pairs" observable in Table 1 and Figure 5 (α_1 and α_2 , α_3 and α_4 , α_5 and α_6 , etc.). Figure 7 shows the parametric relationships between the first six coefficients predicted by the model. The predicted parametric curves closely match the real relationships between the modes, which suggests that the model accurately captures the underlying dynamics of the system.

By substituting the coefficients α_i predicted by the model (equation (5)) into equation (2), we can reconstruct the hawkmoth's wake at any instant during the flapping cycle. Figure 8 shows the predicted wake during the middle of the downstroke (t/T = 0.25). Results are also shown for SINDy models formulated using just N = 2 modes and N = 4 modes. Comparing these predicted wake structures with the real structures in Figure 1(a), we observe that the model improves as more modes are included. We can also see that the leading-edge vortex attached to the hawkmoth's wing becomes more visible as more modes are added to the model.

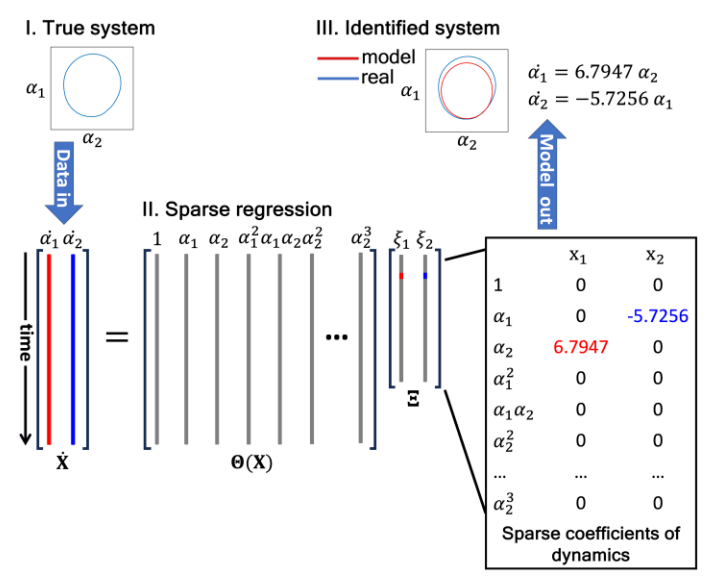


Figure 6. The SINDy algorithm, demonstrated using the first two POD coefficients, α_1 and α_2 . The input data includes the time history X of these coefficients, as well as their time derivative \dot{X} . The candidate function library $\Theta(X)$ includes all polynomial functions of α_1 and α_2 up to order three. Sparse regression is used to find the fewest terms that satisfy $\dot{X} = \Theta(X) \Xi$. The resulting dynamic system is shown and compared against the real dynamics.

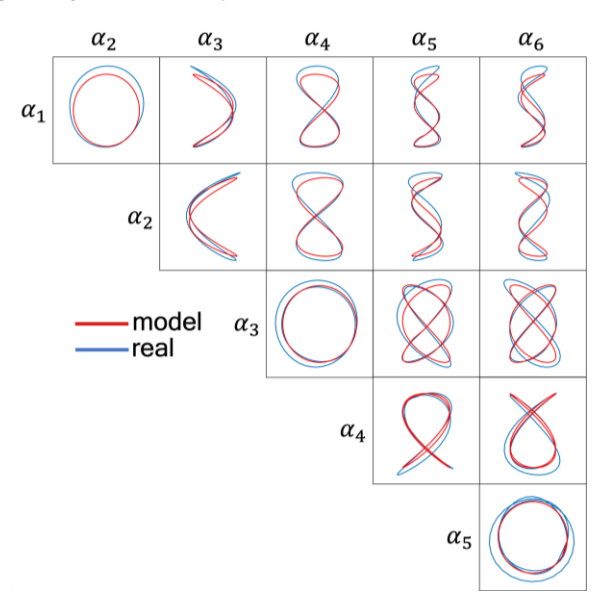


Figure 7. Lissajous curves showing the parametric relationships between the first six POD coefficients (α_1 to α_6). Results are shown for the real coefficients, as well as those predicted by the SINDy model.

To evaluate the accuracy of these various SINDy models (N = 8 modes, N = 4 modes, and N = 2 modes), we use equation (4) to calculate the aerodynamic lift and drag produced by the hawkmoth's wings. Figure 9 shows the predicted forces compared against the real forces from our simulation results. The 2-mode model reflects only the general trend of the hawkmoth's force production. As more modes are included in the model, it better captures smaller fluctuations in force production.

However, there are still significant deviations between the 8-mode model and real force production, most notably during the wing-reversal period around t/T=0. We believe that these discrepancies are due to the complexity and spatiotemporal asymmetry of the hawkmoth's wake (see Figure 1). During the wing-reversal period, it is likely that high-frequency low-energy modes contribute to the hawkmoth's force production. In future studies, we plan to identify and incorporate these contributions into our reduced-order model to improve its accuracy.

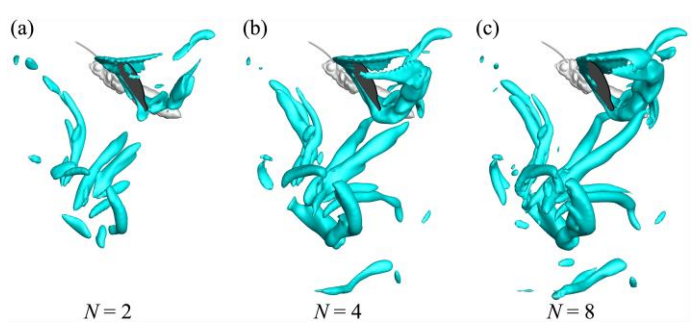


Figure 8. Q-criterion wake structures during the middle of the downstroke (t/T = 0.25). Results are shown for SINDy models created using (a) 2 POD modes, (b) 4 POD modes, and (c) 8 POD modes.

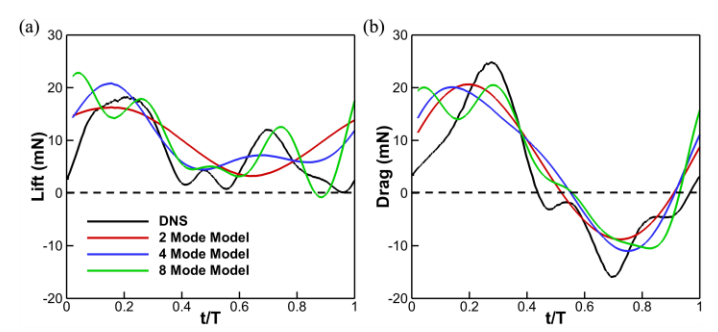


Figure 9. Predicted (a) lift and (b) drag production for the various SINDy models. Results are compared against the real force production from the direct numerical simulation (DNS).

4. CONCLUSION

In this study, we created a reduced order model of a hovering hawkmoth's wake. We first simulated hovering hawkmoth flight using an in-house CFD solver. Then, we decomposed the flow into a set of time-varying POD modes. Using SINDy, we created a reduced order model that relates the 8 most energetic POD modes and accurately predicts the system dynamics. We also found that using less than 8 POD modes to create the model significantly reduces its accuracy. However, there are still some significant errors in the 8-mode model, especially when it is used to predict the hawkmoth's aerodynamic force production. Future plans to improve model accuracy include exploring alternative modal decomposition techniques (e.g., dynamic mode decomposition) and using an autoencoder neural network to further reduce the dimensionality of the system. Reduced order modeling of insect flight has the potential to yield new insights

into flapping-wing propulsion, as well as provide inspiration for the design and control of bio-inspired micro-aerial vehicles.

ACKNOWLEDGMENTS

This work is supported by NSF CBET-2042368 to CL and NSF IIS-1239212 to TLH. All simulations were run on the High-Performance Computing Cluster of the College of Engineering at Villanova University.

REFERENCES

- [1] C. P. Ellington, C. Van Den Berg, A. P. Willmott, and A. L. Thomas, "Leading-edge vortices in insect flight," *Nature*, 384, 626-630, 1996.
- [2] Z. J. Wang, "The role of drag in insect hovering," Journal of Experimental Biology, 207, 4147-4155, 2004.
- [3] D. J. Lucia, P. S. Beran, and W. A. Silva, "Reduced-order modeling: new approaches for computational physics," *Progress in aerospace sciences*, 40, 51-117, 2004.
- [4] J. Burkardt, M. Gunzburger, and H.-C. Lee, "POD and CVT-based reduced-order modeling of Navier–Stokes flows," *Computer methods in applied mechanics and engineering*, 196, 337-355, 2006.
- [5] L. Sirovich, "Turbulence and the dynamics of coherent structures. I. Coherent structures," *Quarterly of applied mathematics*, 45, 561-571, 1987.
- [6] A. Chatterjee, "An introduction to the proper orthogonal decomposition," *Current science*, 808-817, 2000.
- [7] S. L. Brunton, J. L. Proctor, and J. N. Kutz, "Discovering governing equations from data by sparse identification of nonlinear dynamical systems," *Proceedings of the national academy of sciences*, 113, 3932-3937, 2016.
- [8] Y. Guan, S. L. Brunton, and I. Novosselov, "Sparse nonlinear models of chaotic electroconvection," *Royal Society Open Science*, 8, 202367, 2021.
- [9] J. L. Callaham, S. L. Brunton, and J.-C. Loiseau, "On the role of nonlinear correlations in reduced-order modelling," *Journal of Fluid Mechanics*, 938, A1, 2022.
- [10] J.-C. Loiseau and S. L. Brunton, "Constrained sparse Galerkin regression," *Journal of Fluid Mechanics*, 838, 42-67, 2018.
- [11] C. Li, H. Dong, and G. Liu, "Effects of a dynamic trailing-edge flap on the aerodynamic performance and flow structures in hovering flight," *Journal of Fluids and Structures*, 58, 49-65, 2015.
- [12] C. Li and H. Dong, "Wing kinematics measurement and aerodynamics of a dragonfly in turning flight," *Bioinspiration & Biomimetics*, 12, 026001, 2017.
- [13] S. Lionetti, T. L. Hedrick, and C. Li, "Aerodynamic explanation of flight speed limits in hawkmoth-like flapping-wing insects," *Physical Review Fluids*, 7, 093104, 2022.

- [14] Y. Liu, A. D. Lozano, T. L. Hedrick, and C. Li, "Comparison of experimental and numerical studies on the flow structures of hovering hawkmoths," *Journal of Fluids and Structures*, 107, 103405, 2021.
- [15] S. Lionetti, Z. Lou, A. Herrera-Amaya, M. L. Byron, and C. Li, "A new propulsion enhancement mechanism in metachronal rowing at intermediate Reynolds numbers," *Journal of Fluid Mechanics*, 974, A45, 2023.
- [16] C. Li, H. Dong, and K. Zhao, "A balance between aerodynamic and olfactory performance during flight in Drosophila," *Nature Communications*, 9, 1-8, 2018.
- [17] M. Lei and C. Li, "Wings and whiffs: Understanding the role of aerodynamics in odor-guided flapping flight," *Physics of Fluids*, 35, 121901 2023.
- [18] M. Lei, M. A. Willis, B. E. Schmidt, and C. Li, "Numerical Investigation of Odor-Guided Navigation in Flying Insects: Impact of Turbulence, Wingbeat-Induced Flow, and Schmidt Number on Odor Plume Structures," *Biomimetics*, 8, 593, 2023.
- [19] C. Li, "Effects of wing pitch kinematics on both aerodynamic and olfactory functions in an upwind surge," *Proceedings of the Institution of Mechanical Engineers, Part C: Journal of Mechanical Engineering Science,* 235, 296-307, 2021.
- [20] S. Lionetti, T. L. Hedrick, and C. Li, "Numerical investigation of olfactory performance in upwind surging hawkmoth flight," *AIAA Paper 2023-4242*, 2023.
- [21] F. Noca, D. Shiels, and D. Jeon, "Measuring instantaneous fluid dynamic forces on bodies, using only velocity fields and their derivatives," *Journal of Fluids and Structures*, 11, 345-350, 1997.
- [22] C. Li, J. Wang, and H. Dong, "Proper orthogonal decomposition analysis of flapping hovering wings," in 55th AIAA Aerospace Sciences Meeting, 2017, 0327.
- [23] Z. Liang and H. Dong, "Virtual force measurement of POD modes for a flat plate in low Reynolds number flows," in *52nd Aerospace Sciences Meeting*, 2014, 0054.